Proc. PIXEL2002 International Workshop, Carmel, CA, 2002; SLAC Electronic Conference Archive, in press. (Jan. 2003)

Radiation Hardness/Tolerance of Si Sensors/Detectors for Nuclear and High Energy Physics Experiments

Zheng Li
Brookhaven National Laboratory, NY 11973-5000, USA

Abstract

Silicon sensors, widely used in high energy and nuclear physics experiments, suffer severe radiation damage that leads to degradations in sensor performance. These degradations include significant increases in leakage current, bulk resistivity, and space charge concentration. The increase in space charge concentration is particularly damaging since it can significantly increase the sensor full depletion voltage, causing either breakdown if operated at high biases or charge collection loss if operated at lower biases than full depletion. Several strategies can be used to make Si detectors more radiation hard/tolerant to particle radiations. In this paper, the main radiation induced degradations in Si detectors will be reviewed. The details and specifics of the new engineering strategies: material/impurity/defect engineering (MIDE); device structure engineering (DSE); and device operational mode engineering (DOME) will be given.

Key words: Si sensor, radiation, damage, space charge transformation, radiation hardness, radiation tolerance, defect/impurity/material engineering, operational mode.

I. Introduction

Silicon sensors continue to be applied to nuclear and high-energy physics experiments in both increasing complexity and quantity. Large area of silicon sensors as trackers (pixel, strip and drift detectors) are now being built/implemented in ATLAS, CMS, and ALICE detector systems at LHC; CDF, D0 and BTeV at FNAL; and STAR, PHENIX, and PHOBOS at RHIC [1-2]. Si sensors, however, suffer from displacement radiation damages that cause significant degradation in sensor performance. Major among them are: 1) increase of sensor leakage current with radiation fluence, which result in high noise and high power requirement; 2) increase of bulk resistivity with fluence towards the intrinsic value (about 200-300 k-Ωcm); and 3) increase of sensor full depletion voltage with fluence, which causes possible breakdown (if operated at high biases) and/or charge collection efficiency (CCE) loss (if operated at partial depletion). In this paper, the current results on Si sensor radiation degradations will be reviewed and summarized. Two different engineering approaches to improve Si sensor radiation hardness/tolerance: Material/Impurity/Defect Engineering (MIDE) Device Structure Engineering (DSE), and device operational mode engineering (DOME) will be introduced.

II. Radiation Induced Degradations in Si Sensors

1. Displacement Radiation Damage in Si

It is well known that neutrons, protons, electrons, and even gamma radiation can lead to displacement damage in Si. The displacement damage is caused by displacement of a Si atom from its substitution site to an interstitial site to form a Frankel pair, as shown in Fig. 1 for neutron situation. In the case of neutron radiation, due to the high Si recoil energy (133 keV), the displacement damage is a cascade with many interactions, resulting in an extended damage region, or defect clusters [3]. In the case of gamma radiation, however, the displacement damage is caused by the Compton electrons (about 1 MeV in energy) that only produce isolated single defects when vacancies/interstitials react to each other or to impurities in the Si, as shown in Fig. 2. In the case of charged particles, protons, pions, etc., due to Columbic interaction, the displacement damages in Si are partially defect clusters and partially isolated single defects. Therefore, even for the same amount of non-ionizing energy loss (NEIL) in Si, defect structures caused by different radiation particles can be very different. Table I summarizes qualitatively the defect structures caused by different types of radiation particles.

2. Increase in Sensor Leakage Current

Increase of sensor leakage current under radiation is caused by the radiation induced deep level defects that act as generation and recombination centers. These deep levels include V-V (double vacancy center) and V-V relater complexes, P-V or E-center (phosphorus vacancy center), O-V or A-center (oxygen vacancy center) and levels in the

defect clusters. It has been found that the leakage current density, current per unit volume, increases linearly with fluence. For 1 MeV equivalent neutron fluence, $\Phi_{n,\,equ}$. The increase in volume current, ΔJ, can be written as [4]:

$$\Delta J = \alpha \ \Phi_{n,equ}$$

Where α is called the damage constant. The range of α, for high resistivity Si (2-8 kΩ-cm), is within 4-6x10^{-17} A/cm at 20 °C [5]. Since the process of carrier generation via the deep levels is an activated process, the resulting leakage is extremely sensitive to temperature: it decreases exponentially with decreasing temperature. This strong temperature dependence gives rise to the low temperature operation of Si sensors at greatly reduced leakage current. Fig. 3 shows the leakage current dependence on temperature of a neutron irradiated Si sensor and simulated current using two deep levels. It is clear that, a modest cooling from 300 K to –10 °C (263 K) reduces the sensor leakage current by nearly 2 orders of magnitude. The fit to the total current using two deep levels agrees quite well to the experimental data [6].

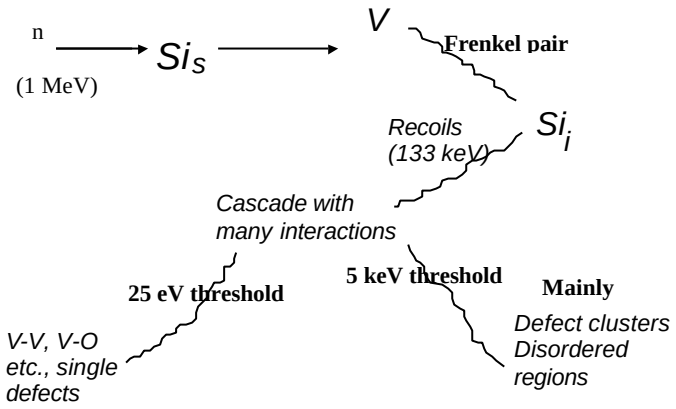

Fig. 1 Primary and secondary defects in Si caused by fast neutrons.

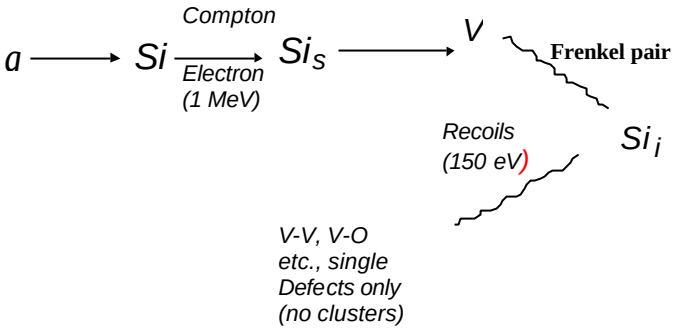

Fig. 2 Primary and secondary defects in Si caused by gamma radiation.

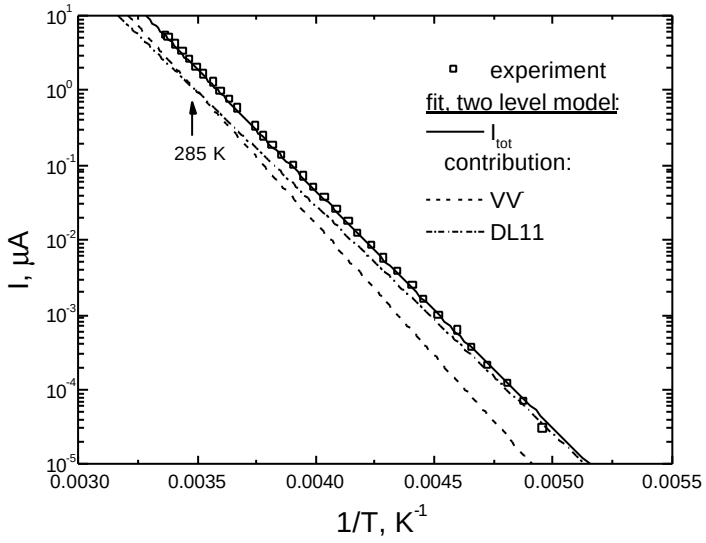

Fig. 3 Leakage current as a function of temperature for n-irradiated Si sensors.

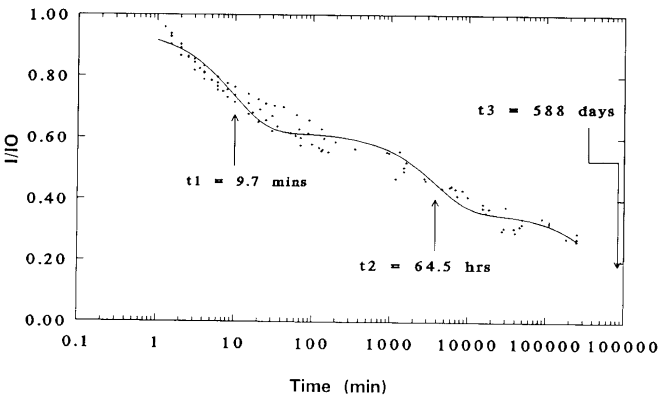

Fig. 4 RT annealing of leakage current in n-irradiated Si sensors.

Table I Different types of defect structures created by different radiation particles. Number of X's is a qualitative indication of the amount.

Particle type	**Single defects**	**Defect clusters**
n	**x**	**xxxxx**
Charged particles (p, *p*, etc.)	**xxxx**	**xx**
g*, *e	**xxxxxx**	

The leakage current can be annealed at RT (room temperature) or at elevated temperatures. Fig. 4 shows the annealing stages at RT of a neutron irradiated Si detectors [7]. Each annealing stage indicates the annealing out of a particular defect level responsible for the sensor leakage current. Extensive modeling and parameterization of leakage current annealing has been done by the Hamburg group [8]. As shown in Fig. 5,

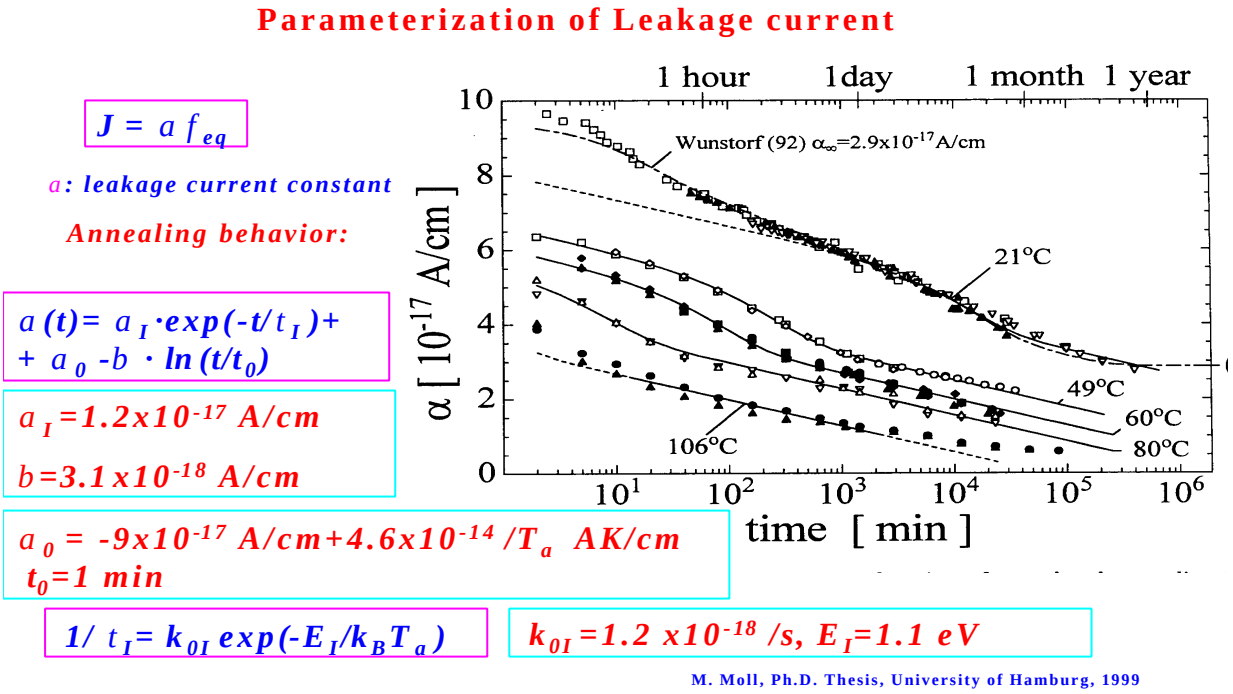

Fig. 5 Detailed parameterization of detector leakage current annealing.

3. Damage in Sensor Electrical Neutral Bulk

When the sensor is not fully depleted, the un-depleted portion is at zero electric field, or neutral condition called electrical neutral bulk (ENB). Radiation induced changes in ENB are mainly in the carrier concentration, bulk resistivity, and carrier low field mobility. Radiation induced deep levels can cause carrier removal and compensation, leading to the dramatic increase in bulk resistivity. Fig. 6 shows the ENB resistivity, obtained from a direct resistor measurement [9], as a function of neutron fluence for n-type Si materials with different resistivity. It is clear that ENB resistivity increases with neutron fluence regardless of Si initial resistivity and type (CZ or FZ). The resistivity will eventually saturate at a value close the intrinsic resistivity, between 200-300 kΩ-cm. This effect is also confirmed by measurement using traditional Hall method [10]. Results in ref [10] also show that p-type Si material behaves similarly with n-type Si, and the carrier Hall mobility degrades with radiation as well. The resistivity saturation with radiation was verified by the measurement of Fermi level position with radiation fluence [11], where Fermi level stabilization near the mid-band gap had been observed at high fluence.

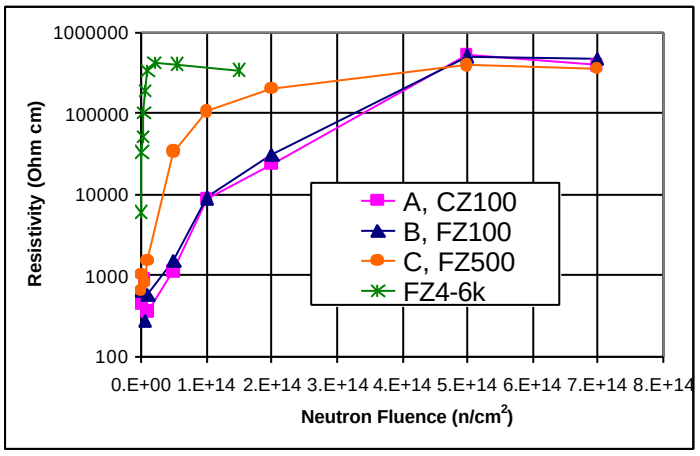

Fig. 6 Changes in Si bulk resistivity with neutron fluence for various starting resistivity.

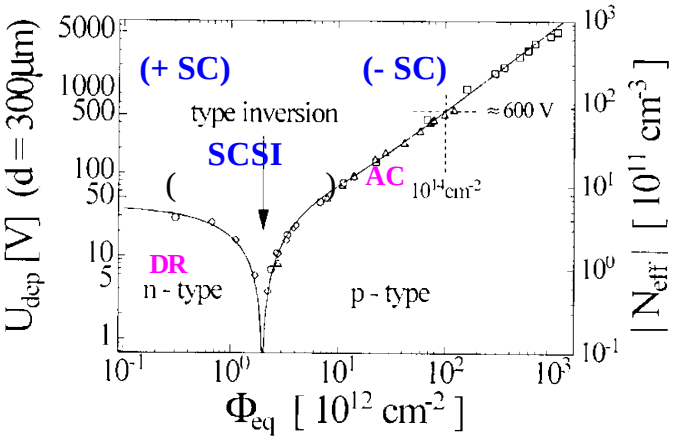

Fig. 7 Changes in Si sensor full depletion voltage and space charge concentration with neutron fluences.

4. Space Charge Transformations and CCE Loss

Si sensors used as particle detectors, typically in the $p^+/n/n^+$ configuration for n-type Si and $n^+/p/p^+$ configuration for p-type Si, are normally operated at full depletion to get large signal to noise ratio and fast read out. Before radiation, when the sensor is biased at full depletion, the entire detector bulk is a space charge region. In this case, the space charge density is equal to the shallow doping concentration (typically phosphorus for n-type, and boron for p-type), and the space charge sign is positive for n-type bulk, and negative for p-type bulk. For high resistivity Si, the typical value for shallow doping concentration is about 10^{12} cm^{-3} or less. After radiation of 10^{13} n/cm^2 (1 MeV neutron equivalent, the same meaning for the rest of the text) or more, the concentration of radiation induced deep level defects can exceed the shallow doping concentration, resulting in the domination of sensor characteristics by the radiation induced deep level defects. One of the main parameter is the space charge concentration that can be entirely dominated by the radiation induced deep level defects.

a) Space Charge Transformation in as-irradiated Si Sensors

For a fully depleted n-type Si sensor under radiation, the space charge sign undergoes a transformation from initially positive, to negative, termed as the space charge sign inversion (SCSI). This SCSI is caused by two processes: the donor removal (DR) and acceptor creation (AC). Fig. 7 shows the data of the absolute value of the space charge concentration ($|N_{eff}|$) as a function of neutron fluence [12]. This space charge transformation in as radiated Si sensors can be described as the following:

$$N_{eff} = N_{d0} \cdot e^{-g\,\Phi_n} - b\,\Phi_n \cong -b\,\Phi_n \quad (\text{for } \Phi_n \geq 10^{14}\ \text{n/cm}^2) \tag{1}$$

where N_{d0} is the initial shallow doping concentration, g the donor removal rate, and b the introduction rate for deep acceptors. The first term in Equ. (1) is DR, the second term is AC. Note that the parameter N_{eff} has been given a sign freedom: at zero or low fluences, it is positive, and at high fluences, it is negative and dominated by the AC term. The specific fluence at which N_{eff} becomes zero is called the SCSI fluence, or F_i. The SCSI fluence has been found proportional to the initial shallow doping concentration (N_{d0}) of n-type Si sensor, and this leads an N_{d0} dependent donor removal rate, i.e.:

$$g = a / N_{d0} \tag{2}$$

as described in ref. [9] in a modified model. The typical value for a is about 0.1. This N_{d0} dependent doping removal rate may be a result of a possible partial removal of shallow donors [8].

Since sensor full depletion voltage (V_{fd}) depends linearly on the absolute value of the space charge concentration:

$$V_{fd} = \frac{ed^2|N_{eff}|}{2e\varepsilon_0} \cong \frac{ed^2 b}{2e\varepsilon_0} \cdot \Phi_n \quad (\text{for } \Phi_n \geq 10^{14}\ \text{n/cm}^2) \tag{3}$$

where d is the sensor thickness, ε_0 the permitivity for vacuum, and e the permitivity for Si, and it increases nearly linearly with fluence at high fluences, at a given operational bias, the detector may become partially depleted at high fluences. Since the typical value for b is about 0.024 cm^{-1} [13], for a 300 μm thick Si sensor, V_{fd} will increase to 173 volts after being irradiated to $1x10^{14}$ n/cm^2, much larger than the typical initial operation voltage of about 100 volts. This partial depletion will lead to partial collection of charges caused by minimum ionizing particle (MIP) passing through the sensor, and decrease in sensor CCE. High bias voltage operation may bring the sensor back to full depletion mode, however, without special, precautionary measures such as multi-guard-ring design, it may lead to the high field breakdown of the sensor and or high power requirement and thermal runaway. As modeled in ref [14], the detector CCE is affected by two components: the geometry factor that is related to the detector depletion depth as stated above, and the trapping factor that is related to charge trapping by shallow level. The trapping factor can be characterized by a trapping time constant,$\tau_{tre,h}$,(e for electron and h for hole) that is proportional inversely to the trap level density (or radiation fluence). There are many ways of obtaining this trapping time constant: 1) direct way of measuring loss of charges (ΔQ) generated by a well calibrated alpha source, obtaining directly the trapping time constant in the process using $\Delta Q/Q_0 = ½\ t_{ce,h}/\tau_{tre,h}$ (where is the total generated charge, and $t_{ce,h}$ is the collection time for electrons or holes)[15-16], and 2) indirect way of extracting trapping time constant with a new method, introduced by Chilingarov and Kramsburg [17-18]. In this method, a time exponential term with a trail trapping time constant is used

to compensate a similar exponential term caused by trapping in the current pulse shape, thus in the process correct the current pulse shape to a state as if there is no trapping, with a "corrected charge", by integrating the current pulse shape, for each trail trapping time constant. A correct $\tau_{tre,h}$ is determined when the "corrected charge" is not changing with bias voltages > V_{fd}. Details of the new method can be found in ref. [19-22], where a small variant of the method is also described [20-22].

b) Space Charge Transformation with Annealing Time and Temperature

It has been found that, the Si sensor space charge undergoes profound transformation at RT and elevated temperatures even after radiation being stopped. Fig. 8 shows the sensor annealing behavior at RT after neutron radiation to a fluence of $1x10^{14}$ n/cm^2 for Si sensors processed at different conditions [23]. The sensors had all gone through the SCSI, and the normal annealing, termed as beneficial annealing, did occur within the first 10 days after radiation. During this period, the detector full depletion voltage decreases with annealing time, indicating a decrease in the absolute value of the space charge concentration. However, the sensor full depletion voltage starts to increase again after about 10 days annealing at RT. For those sensors shown in Fig. 8, the space charge was negative and became less negative during the beneficial annealing period. After 10 days annealing at RT, the space charge became more negative. This increase of negative space charge was confirmed by the transient current technique for neutron irradiated Si sensors annealed at elevated temperature [24], and was termed as the "reverse annealing". Fig. 9 shows the elevated temperature annealing of Si sensors irradiated by 1 MeV neutrons to various fluences [25]. The reverse

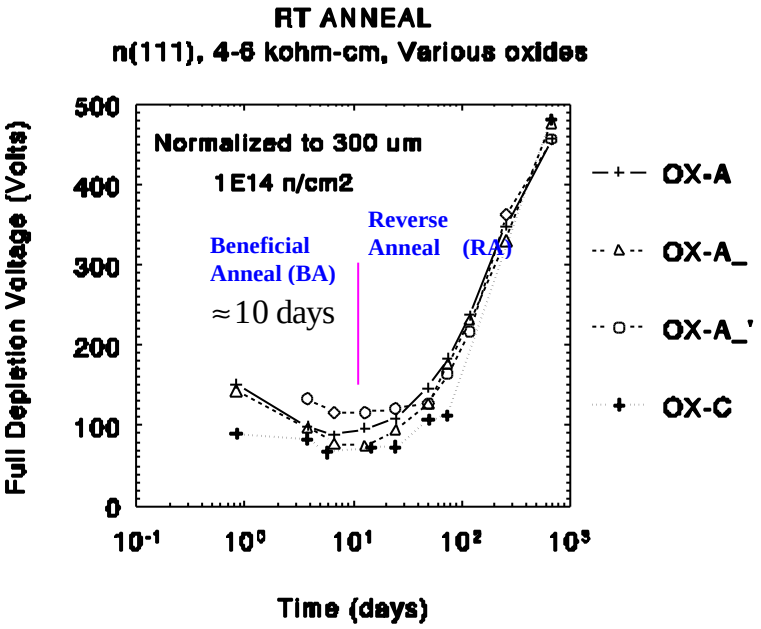

Fig. 8 Beneficial and reverse annealing at RT in irradiated Si sensors fabricated from various thermal processes.

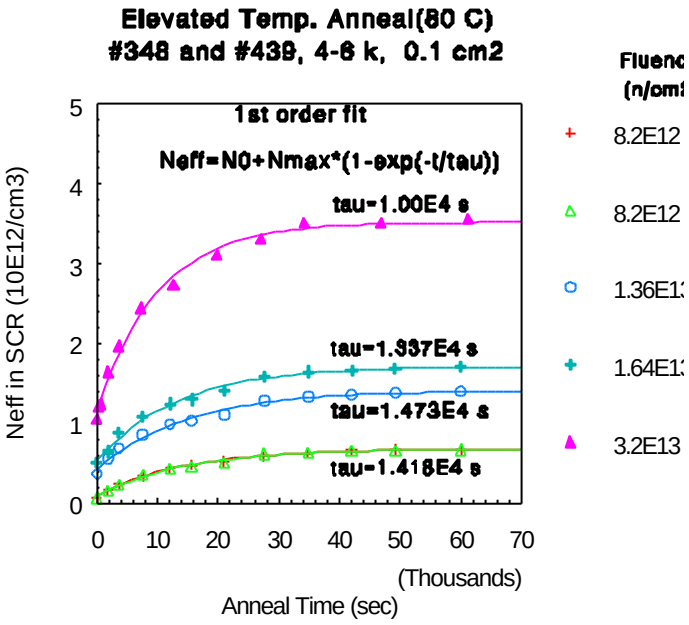

Fig. 9 Reverse annealing at elevated temperatures for Si sensors irradiated to various fluences.

annealing process can be fitted to a first order process with multiple stages [25]. The one-stage first order fit is an average approach that gives practical parameters. Fittings to data in ref. [23,25] give the following:

$$N_{eff}(t,\Phi_n) = N_0(\Phi_n) + N_{eff}^{r,\max}(\Phi_n)\cdot(1-e^{-t/t(T)}) \qquad (4)$$

where $N_0(F_n)$ is the initial space charge concentration before reverse annealing, $N_{eff}^{r,\max}(F_n)$ the amplitude of reverse annealing (2nd term in Equ. (4)), and $t(T)$ the reverse annealing time constant at a given temperature (T). The values of $N_0(F_n)$ and $N_{eff}^{r,\max}(F_n)$ are proportional to the fluence (1 MeV neutron equivalent) [25]:

$$N_0(\Phi_n) = -0.035\cdot\Phi_n \quad ; \quad N_{eff}^{r,\max}(\Phi_n) = -0.073\cdot\Phi_n \qquad (5)$$

and the reverse annealing process is an activated process [23]:

$$t_{1/2}(T) = t(T) \cdot \ln 2 = \frac{1}{n} \cdot e^{\frac{E_a}{kT}} \quad (6)$$

where $t_{1/2}(T)$ is the time constant at which the reverse annealing reaches half of its amplitude, n = 1x10^{13} /s is the jumping frequency, and E_a =1.18 eV is the activation energy.

It is clear that reverse annealing contributes significantly to the total space charge concentration. However, since it is an activated process, it is beneficial to operate the Si sensor at low temperatures to freeze out the reverse annealing. Table II lists the reverse annealing time constant at various temperatures. While it takes less than one year for reverse annealing to take place, it can be delayed to about 15 years at modest cooling to 0 °C. Si sensors to be used in LHC experiments are all planned to be operated at –10 °C to –20 °C.

The mechanism of reverse annealing is believed to be related to the transformation of defect clusters during annealing [26]. During the reverse annealing period, defect clusters begin to break up, releasing single acceptor-like defects to the space charge region, which causes the further increase in negative space charges. This model is consistent with the observation that, for gamma irradiated Si sensors where there is no defect clusters, there is no reverse annealing effect [26].

Table II Reverse annealing time constant at various temperatures.

T (°C)	**-10**	**0**	**20**	**80**
t	**96.8 yr**	**14.6 yr**	**179 d**	**3.7 hr**

For practical LHC applications, lots of efforts have been directed into parameterization of the space charge transformation process. Fig. 10 shows the Hamburg model that deals with all parameters regarding the space changes during radiation (as-irradiated) and anneal [8]. The changes of space charge, ΔN_{eff} , is divided into three components: the beneficial annealing N_A , the stable defects N_C , and the reverse annealing N_Y . As shown in the figure, each component is modeling in detail with parameters derived from the experimental data. Note here that, although the reverse annealing is modeled by a second order process, a fluence dependent time constant was used, which implies the underlining first order process as stated before.

However, the above presented results were obtained from the pad detectors with larger area to perimeter ratio (≥ 0.1 cm). For segmented detectors in real experiments, this ratio can be as small as 5x10^{-3} cm, which can introduce surface effect related geometric effects that may affect the detector performance. Also, the real detector operation conditions (low temperatures, under large reverse bias, etc.) may also affect the detector performance. Recently, Casse has presented some preliminary date on the CCE of ATLAS microstrip detectors as a function of proton ration dose for Si detectors made on different materials [27]. One surprise there is that there seems no difference between standard detectors and supposedly radiation hard oxygenated detector (as we will see in the next section). Cindro et al. has performed annealing test of irradiated Si detector under operational biases [28-30]. In these studies, a damage component related to the bias operation has been found, which exhibits a bistable behavior upon bias re-application. The Karlsruhe group has done extensive studies on the Lorentz angle of charges drifting in both electric and magnetic fields for microstrip detectors at temperatures from RT down to cryogenic temperatures [31-34].

C) Space Charge Transformation due to Free Carrier Trapping (Space Charge Manipulation)

It has been observed that, for irradiated Si sensors, the space charge can be affected by the trapping status of free carriers injected into the sensor. In 1995, Eremin et al. first reported the space charge transformation by laser induced free electrons and holes [35]. In this paper, it has been observed that hole trapping by radiation induced deep levels can cause the space charge sign “re-inversion”: from its already inverted state of negative sign to positive after trapping of free holes introduced by laser. The space charge, both sign and concentration, can be therefore manipulated by injected free carriers. Data shown in Fig 11 come from direct measurements of space charge with temperature for both hole trapping and electron trapping [36]. The space charge was initial negative at RT (300K), which was resulted from the radiation induced SCSI. With hole trapping, the space charge sign was re-inverted from negative to positive at about 150 K. For electron trapping, however, the space charge went more negative at about 155 K. The three transition temperatures associated to the three steps in space charge transformations are identified to be related to three deep levels: two for hole trapping, and one for electron trapping [36]. In an ideal situation, one may manipulate the space charge concentration in such a way that its concentration is minimum, thus greatly reducing the sensor full depletion voltage. At a given voltage, the reduction in space charge concentration results in the increase of the depletion depth, leading to an increase in the sensor CCE. In fact, late measurements on sensor CCE of charges created by laser have

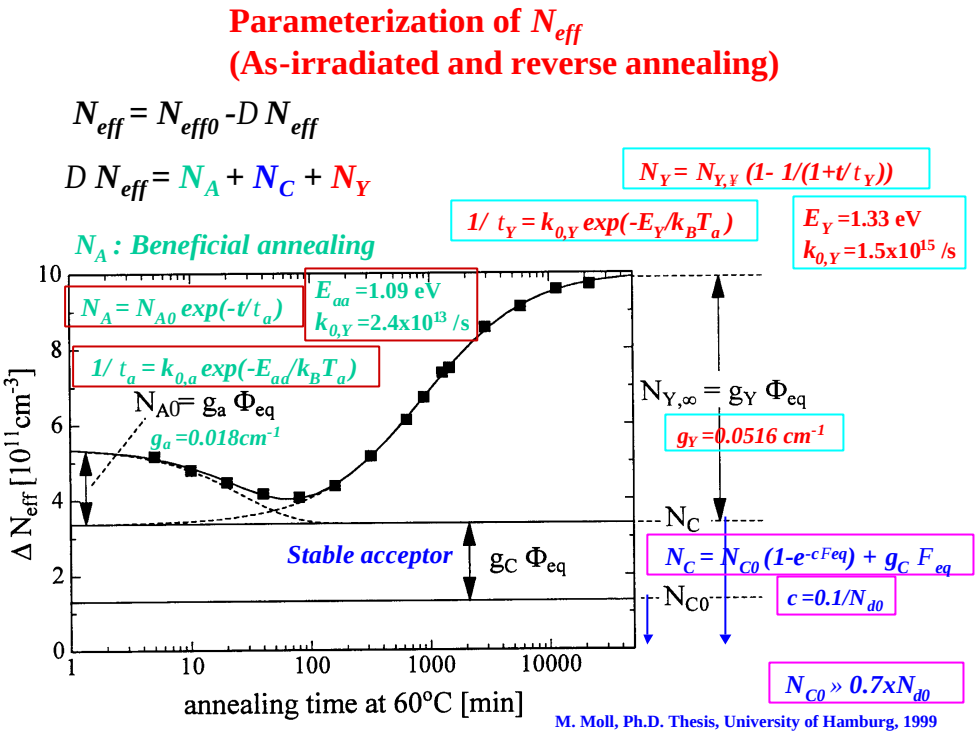

Fig. 10 Detailed Parameterization of the space charge transformation during radiation and anneal.

shown significant increase in sensor CCE with trapping of free holes at cryogenic temperatures [14]. We note here that free carrier injection can be produced by laser, current (injection current, thermal generation current, current caused by passing particles, etc). Fig. 12 shows that, at a given cryogenic temperature, an optimal electric field distribution can be achieved in a Si sensor by adjusting the injection current density to an optimal value, typically in the order of 10's of nA [37]. However, with large enough injected carrier concentration/current, one can even achieve minimum/optimal space charge concentration even at or near RT [38].

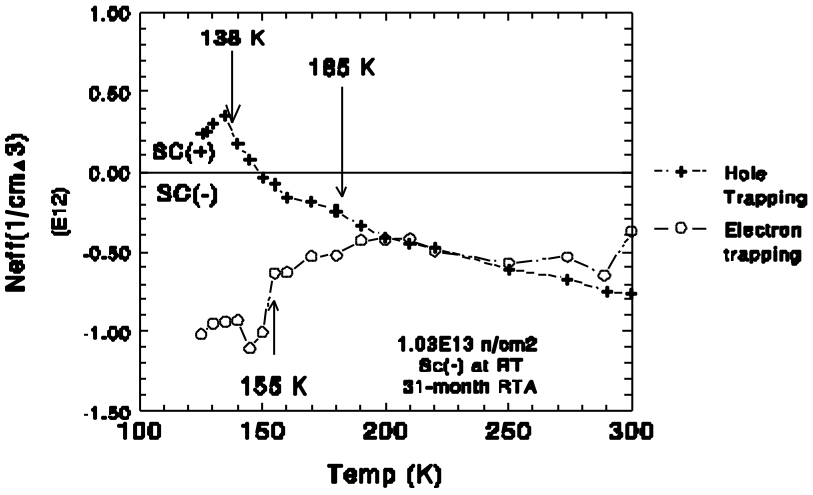

Fig. 11 Free carrier trapping induced space charge changes in irradiated Si sensor at cryogenic temperatures.

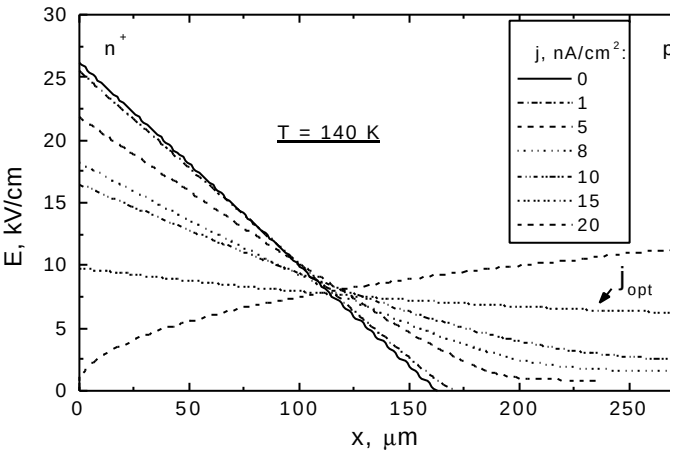

Fig. 12 Simulated electric field distribution in irradiated Si sensor at various current injection conditions.

The so-called Lazarus effect, the recovery of CCE in heavily irradiated Si sensors at cryogenic temperatures, have been discovered in 1998 [39], and it has been one of the main subjects for the CERN RD39 Collaboration [40]. Readers who are interested in more details of the Lazarus effect and radiation hard cryogenic Si detectors are referred to ref. [39-42].

D) Double Junction/Double Peak Electric Field Distribution

In 1992, we have observed in heavily irradiated $p^+/n/n^+$ Si detectors an abnormal electric field distribution deviating from its normal linear form. It has been found that, after being irradiated much beyond the SCSI, alpha particle induced current pulses can be seen from both sides of the detector that is not fully depleted, implying existence of a junction on either side of the detector [43]. This effect is also called the double junction (DJ) effect. A qualitative model with two deep levels, one donor level for the positive space charge near the p^+ contact, and one acceptor level for the negative space charge near the n^+ contact was proposed in ref. [43], as shown in Fig. 13. This abnormal electric field distribution in heavily irradiated Si sensors has been confirmed later in fully depleted sensor, where double peaks (DP) in current pulses induced by red lasers have been clearly seen [35, 44]. Fig. 14 [44] shows the current pulse shapes induced by red laser illuminating on the p^+ contact, which produces electron current drifting from the p^+ contact to the n^+ contact. Since the current is nearly proportional to the electric field, a DP distribution in current indicates the same in the electric field distribution.

Recently, Eremin et al have made extensive modeling on the DJ/DP effect [45]. It has been concluded that the physics for DJ and DP is the same, only when the bias is less than full depletion, the DJ effect is seen, and when the bias is greater than the full depletion, the DP effect is seen. Fig. 15 shows the results from the detailed modeling on the DJ/DP effect, which has clearly demonstrated the abnormal electric field distribution under various bias voltages [45]. Two deep levels, one deep donor and one deep acceptor, have been used in the modeling, for which the parameters are shown in Table III [45]. It is clear that, the abnormal electric field distribution in heavily irradiated Si sensors can cause problems not only in sensor operation, but also in the traditional modeling of sensor electrical properties, where a linear electric field has been widely accepted and used.

III. Radiation Hardness of Si Sensors

1. Material/impurity/defect Engineering (MIDE)

Material can be made more radiation hard by introduction of known impurities in the material purposefully. The known impurity introduced into the material, under the condition it will not significantly alter the material properties, can interact with the primary defects caused by radiation, vacancies and interstitials, to form such defect complexes that are much less damaging than the more intrinsic defects (V-V, high order V complexes, and defect clusters). The role of theses known defects is to getter the radiation-induced primary defects. Detail modeling of defect kinetics has shown effectiveness of surplus oxygen in Si detectors in suppressing the formation of deep V-V and V_2O detects [46-47].

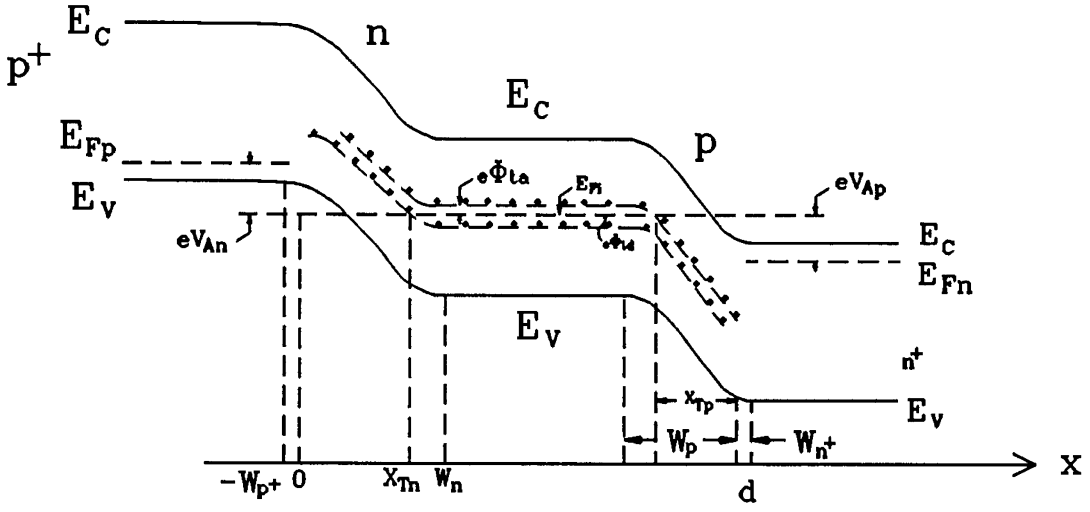

Fig. 13 Energy band diagram for the proposed two-level model for the double junction effect.

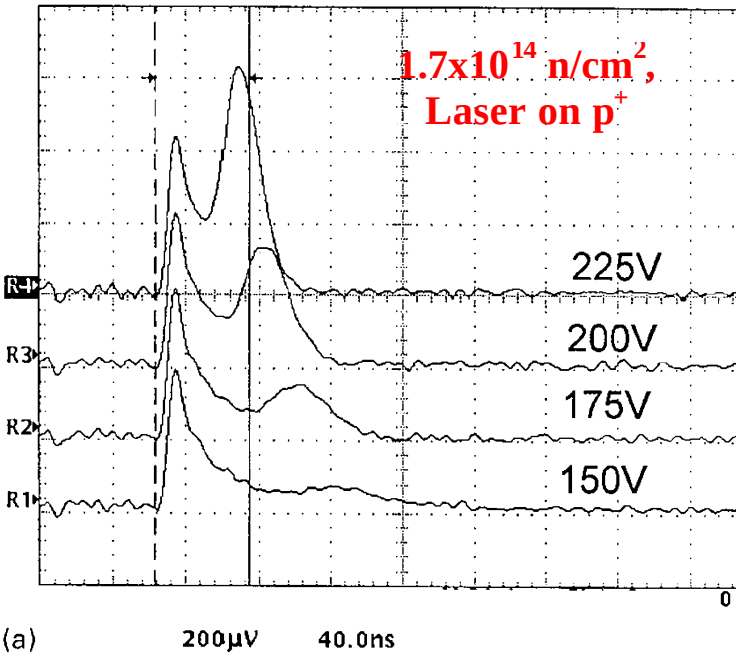

Fig. 14 Red laser induced electron current shapes for irradiated Si sensors biased at various voltages. Double peaks in current shapes are clearly seen.

In 1992, BNL has developed a safe and reliable way of introducing oxygen into Si during the oxidation process [48]. The process, named High-temperature, long-time (HTLT) oxidation, is a small alternation from the conventional processing of high resistivity Si detectors. In the HTLT oxidation process, Si wafers are oxidized at 1150 °C to 1200 °C in an oxygen ambient for over 24 hours, resulting in an oxygen concentration over a few times of 10^{17} /cm^3 uniform over 50 µm depth from either side of wafer. However, test results on these HTLT Si detectors to fast neutron radiation had shown no improved radiation hardness as compared to standard Si detectors [23].

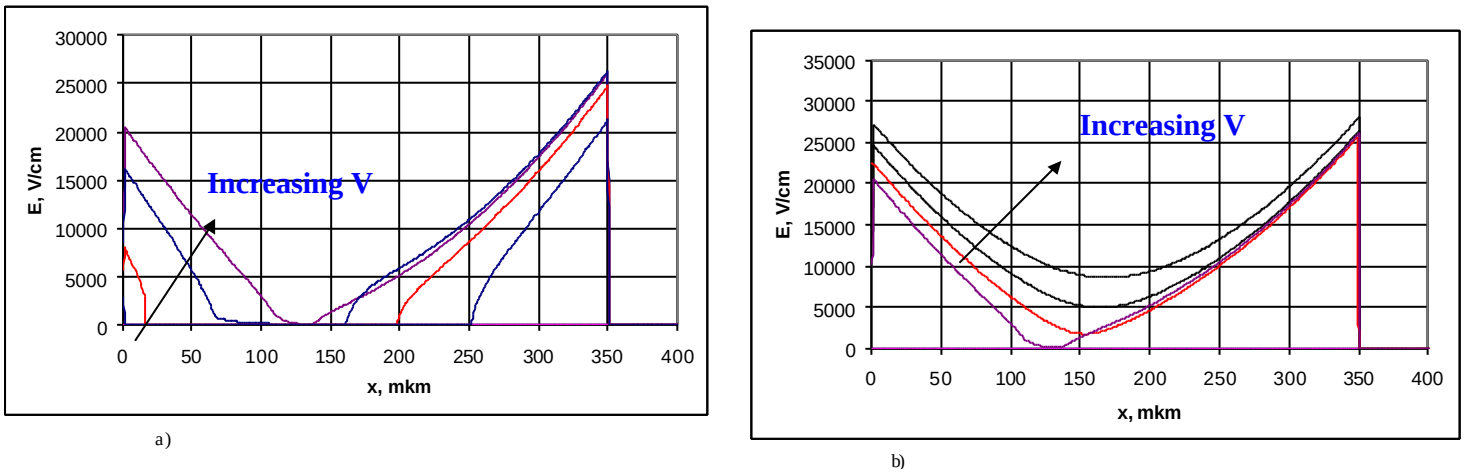

Fig. 15 Simulated electric field for heavily irradiated Si sensors a) at lower biases that the full depletion voltage (DJ); and b) at higher biases than the full depletion voltage (DP).

Table III Parameters for deep levels used in the modeling of DJ/DP effect

DL #	Ci-Oi		Deep donro		V-V		Deep acceptor	
D/A, 0/1	0		0		1		1	
	electrons	holes	electrons	holes	electrons	holes	electrons	holes
Et=Edl-Ev	0.36	#REF!	0.52	#REF!	0.7	-0.7	0.6	-0.6
sig/e[cm2]	1.00E-15		1.00E-15		1.00E-15		1.00E-15	
sig/h[cm2]		1.00E-15		1.00E-15		1.00E-15		1.00E-15
Ndl[cm-3]	0.00E+00		4.60E+14		0.00E+00		4.00E+15	

In the time period of 1999-2000, in the interest of developing radiation hard Si detectors for LHC, where charged particles (protons, pions, etc) dominate, renewed interest had been generated to develop oxygenated Si detectors: 1) under the frame work of CERN RD48 Collaboration, a technology called Diffused Oxygen Float Zone Si (DOFZ Si) was developed that oxidize Si wafer at high temperature (1150 °C) for short period of time (a few hours) then drive-in (via diffusion) the oxygen in to the Si bulk in a N_2 ambient at the same high temperature [49-52]; and 2) BNL had advanced its HTLT technology with even longer oxidation time (9 days) at 1200 °C to obtain uniform oxygen concentration of about $4x10^{17}$ /cm^3 over the entire 300-400 μm thickness, with and without thermal donor (TD) [53]. Although again no radiation hardness to neutron radiation was observed, oxygenated Si detectors by either DOFZ or HTLT technology have been found more radiation hard to charged particle radiation (proton and pion) [49-53]. Fig. 16 [49, 53] shows that, as compared to standard Si detector, the beta (β see Eq. (1)) value is reduced by more than a factor of 2 in oxygenated Si detectors. Note that, for HTLT(TD) Si detectors, there is a wide flat range for beta (beta zero region) due to the fact that TD's are not removed by radiation. More interestingly, it has been found that oxygenated Si detectors are almost insensitive to gamma radiation up to 600 Mrads, as shown in Fig. 17a [53]. While standard Si detectors have gone through the normal SCSI due to negative space charge build up caused by gamma radiation, the full depletion voltage of oxygenated Si detectors has hardly changed. In fact, most resent data has shown that (Fig 17b, ref [54]), up to a dose of close to 2 Grad, there is a monotonical small build up of positive space charge in oxygenated detectors [54-55].

A model has been proposed by BNL (BNL Model) that explains the difference in oxygen effect to different radiation source [43, 56]. As shown in Fig. 18, and explained in Section II.1, for neutron radiation, there are mostly defect clusters where the local ratio of [O]/[V] can be very small (<<0.1), preventing an effective gettering of V's by oxygen; while for gamma radiation, there are mostly point defects that are uniformly distributed in Si, the ratio of [O]/[V] >>1, and the oxygen gettering effect is maximum. For charged particles, it is somewhere in between, and partial improvement of radiation hardness is observed. Simulations, done by Huhtinen [57], of defect formation in Si for various radiation sources has indeed shown that vacancies are mostly clustering in neutron irradiated Si, for proton radiation, there are mixture of single vacancies and vacancy clusters. Recent DLTS results by Pintilie et al. have shown that, in standard Si detectors irradiated by gamma ray, there are almost one to one correlation between measured concentration of deep level defects (V-V, V_2O or other V-related defects) and the detector leakage current and space charge concentration [58-59]. In oxygenated Si detectors, both the leakage current and space charge concentration introduction rates were much lower, indicating that both V-V and V_2O deep level defects are greatly suppressed due to oxygen effect, in agreement with simulation results in ref [46-47] and the proposed model.

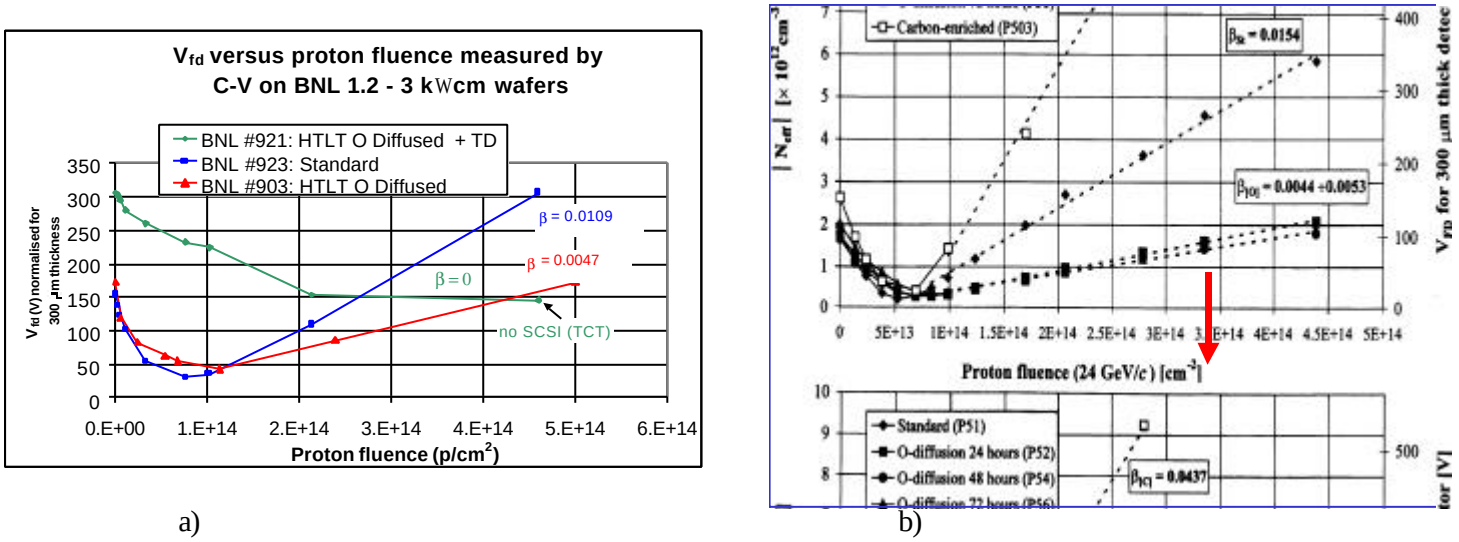

a) b)

Fig. 16 Changes in full depletion voltage and/or space charge concentration as a function of 24 GeV proton fluence for oxygenated Si detectors as compared to standard Si detectors: a) HTLT and HTLT(TD) detectors; and b) DOFZ detectors.

2. Device Structure Engineering (DSE)

As explained in Section II.4, the main electrical degradation that affects Si detector operation most is the increase in detector full depletion voltage due to the negative space charge build up during radiation and during the RT storage (annealing). Major efforts have been made to improve the detector radiation tolerance by 1) increase the detector breakdown voltage using multi-guard rings; 2) decrease the detector full depletion voltage using novel

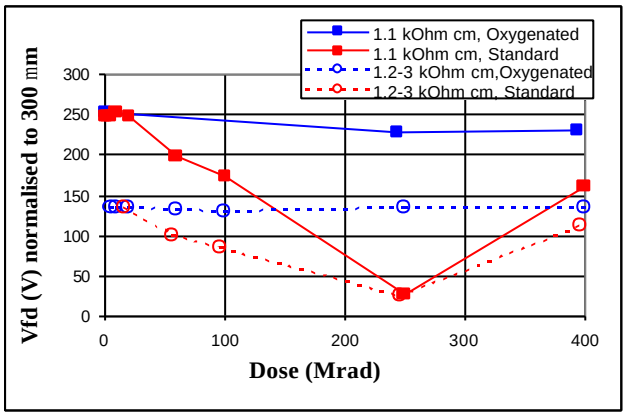

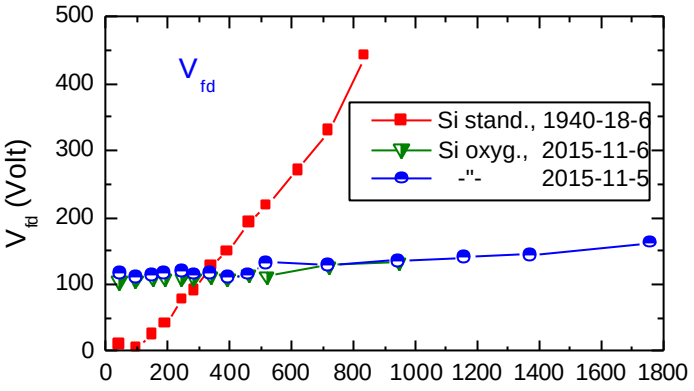

a) b)

detector structures (3D and Semi-3D detectors); and 3) decrease the detector full depletion voltage using thinner detectors.

Fig. 17 Changes in full depletion voltage as a function of ^{60}Co gamma dose for HTLT oxygenated Si detectors as compared to standard Si detectors: a) early results at low doses; and b) recent results at high doses close to 2 Grad.

a) Multi-guard Ring System

Use of multi-guard ring system can redistribute the electric field over a larger distance along the detector edge, thus preventing break down along the detector edge at large bias voltages. The detector is thus operated at much larger biases than the initial full depletion voltage, and can tolerate larger radiation fluence before the detector is forced into partial depletion by radiation-induced negative space charge build up [60-62]. Fig. 19 shows the breakdown characteristics of $n^+/p/p^+$ Si detectors with different number of guard rings [62]. The initial full depletion voltage is about 100 volts. It is clear that, with 7 or more guard rings, the breakdown voltage can be pushed close to 1000 volts, for which an equivalent fluence of $6x10^{14}$ n/cm^2 can be tolerated.

In almost all experiments at LHC, multi-guard ring system has been used for Si strip and pixel detectors. Some even adapted the $n^+/n/p^+$ structure that has segmented electrodes on the n^+ side. In this case, after SCSI when the junction is shifted to the n^+ side, the detector may be still operational at partial depletion mode at very high radiation fluences.

Model for the role of oxygen in rad-hardness

Particle type	Single defects	Defect clusters	Oxygen effect
n	x	xxxxxx R_{V-V}>>1	No
Charged particles (p, *p*, etc.)	xxxx R_{V-V} <<1	xx	Partial
g	xxxxxx R_{V-V} <<1		Yes

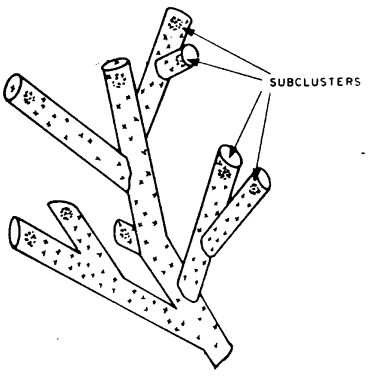

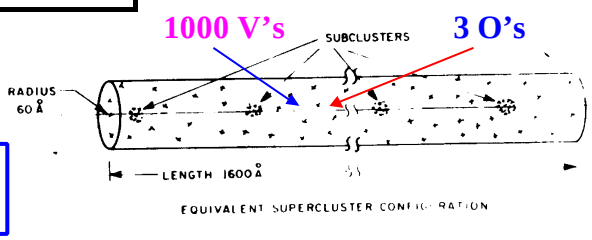

The local [O] is much smaller than [V] within the cluster

Z. Li et al., Nucl. Inst. & Meth., A461 (2001) 126-132

Fig. 18 BNL model for the difference in oxygen effects to different types of radiations.

b) 3D Detectors

Developed by Park at University of Hawaii [63], the 3D detector got its name from the way it is processed. Different from conventional planar technology, p^+ and n^+ electrodes are diffused in small holes along the detector thickness ("3-d" processing), as shown in Fig. 20. The depletion develops laterally between the p^+ and n^+ electrodes that can be made 50 to 100 μm in separation. The detector full depletion voltage thus just depends on the p^+-n^+ separation, and it is insensitive to detector thickness. Since this separation can be made very small (<100 μm), much less voltage will be used to fully deplete the detector, therefore providing much higher radiation tolerance at much lower biases. Fig. 21 shows that the 3D detector can be fully depleted at about 100 volts even after $1x10^{15}$ p/cm^2 55 MeV proton radiation, which provides a factor of 8-10 in full depletion voltage reduction as compare to conventional planar Si detectors.

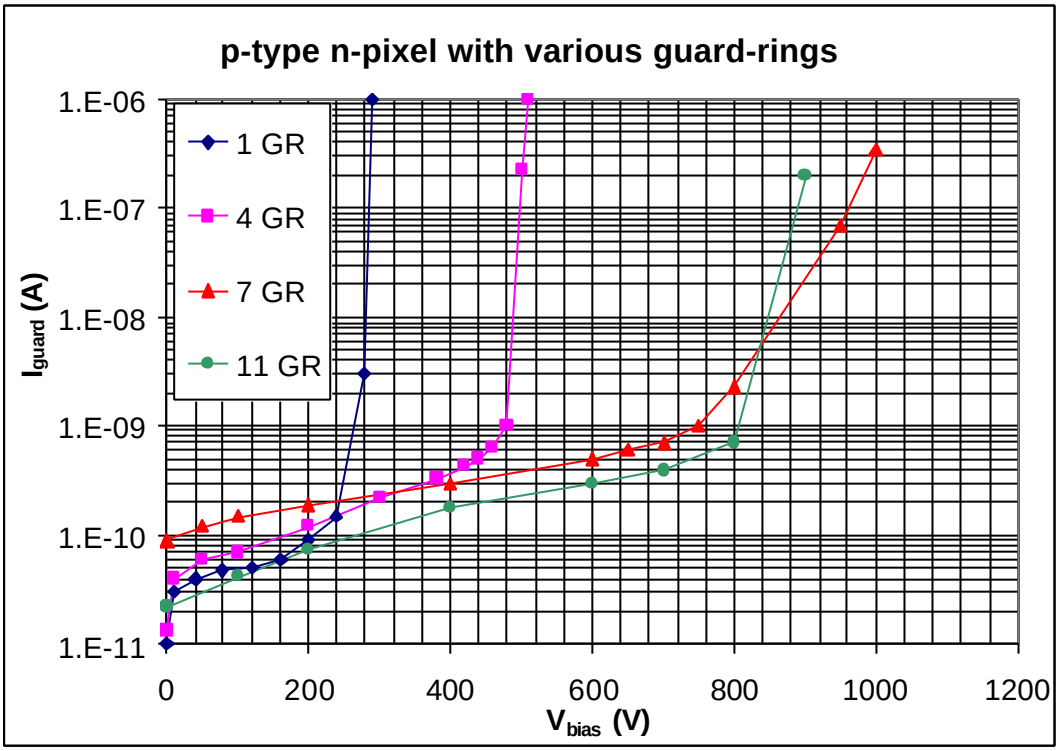

Fig. 19 Current breakdown characteristics for $n^+/p/p^+$ detectors with various guard ring systems.

c) Semi-3D Detectors

Stimulated by the lateral depletion nature of the 3D detectors, the novel idea of Semi-3D detectors was first developed by BNL in 2000 [64]. As shown in Fig. 22 for a p^+-$n^+/n/n^+$ Semi-3D Si strip detector, both p^+ and n^+ strips are implemented on the front side. The backside is again a uniform n^+ implant. We note here that, although a strip detector example is shown here, this new detector structure can be used also for other segmented detectors such as pad and pixel detectors. The semiconductor substrate can also be materials other than Si, such as Ge, GaAs, CdTe, InN, SiC, diamond, etc. In this novel structure, all the n^+ strips are tied up together to a positive bias that can be smaller or equal to the positive bias on the back n^+ plane, depending on the application needs. Each p^+ strip is connected to an electronics channel for signal readout. Before SCSI, the depletion go both vertically from p^+ strips to the back n^+ plane, as in the conventional single-sided strip detectors, and laterally from p^+ strips to the neighboring n^+ strips. Since the depletion, originated from p^+ strips, has to go both vertically and laterally before SCSI, the full depletion voltage will be higher than a conventional single-sided $p^+/n/n^+$ strip detector, typically by 20%, as shown in Fig. 23. As the radiation goes, before the SCSI, the overall full depletion will go down due to the combined effect of donor removal and acceptor creation, as discussed in Section II.4.a. The nature of depletion still stays the same. However, when the radiation reaches the point beyond the SCSI, there is a dramatic change in the nature of depletion: the depletion now originates from both the n^+ strips in the front side, and the n^+ plane from the backside to the p^+ readout electrodes now being the Ohmic strips. The detector is basically depleted from both sides, thus dramatically decreases the full depletion voltage. In theory, this reduction in full depletion voltage for the same thickness, as compare to the one side depletion in the case of single or double-sided Si strip detectors, should be a factor of 4.

However, as shown in Fig. 24, due to the fact that the front n^+ strips also originate the depletion laterally to the neighboring p^+ strips, which slows down the vertical depletion, the actual reduction factor is about 3 (V_{fd} from 370 volts for ordinary $p^+/n/n^+$ strip detectors with the same thickness and geometry down to 130 volts for the novel detector).

The advantages of this novel p^+-$n^+/n/n^+$ Semi-3D detector structure are: 1) still planar technology, much easier to process than the 3D detector structure; 2) single-sided processing; and 3) it uses the SCSI to our advantage to get an reduction in detector full depletion voltage by a factor of 3 or more.

A small variant of the novel p^+-$n^+/n/n^+$ Semi-3D detector structure is to use p-type substrate, the p^+-$n^+/p/n^+$ Semi-3D detector structure. In this case, it works like the p^+-$n^+/n/n^+$ Semi-3D detector structure after SCSI. The main disadvantage of these types (p^+-n^+/n(or p)/n^+) detector structures is that one can only use the p^+ strips as the readout electrodes, which are (for p-substrate) or become (for n-substrate) the Ohmic electrodes after SCSI.

There are some other variants of Semi-3D detector structures, as proposed in ref. [64]. One of them is a structure that puts $p^+$and n^+ strips/pixels on both sides of the wafer (p^+-n^+/n/ p^+-n^+), thus providing a situation of depletion from both sides before and after SCSI with much reduced full depletion voltage. The advantages of these types of detector structures are: 1) depletion from both sides in any situation; 2) p^+ (and n^+) strips on the front side can be aligned (symmetrical) or misaligned, still parallel (asymmetrical) to those on the backside to created more favorable depletion situations that may reduce the full depletion voltage by a factor of 2 or more; 3) p^+ (and n^+) strips on the front side may be placed with a stereo angle ($0 < \theta \leq 90°$), thus crating a double-sided detector with two dimensional position sensitivity and much reduced full depletion voltage; and 4) in the previous three configurations, either the p^+ strips or the n^+ strips can be used as the readout electrodes, thus giving us a choice to favor the n^+ strips as readout electrodes to gain more radiation hardness even at partial depletion mode The main disadvantage though is that it is a complicated and more expensive double-sided process with p^+ and n^+implants on both sides of the wafer. Another variant is using low resistivity n-type Si substrate (e.g. CZ 100 Ω–cm) with a p^+-n^+/n (low resistivity)/p^+ Semi-3D detector structure that depletes from both side before SCSI. In this case, it will work at least to the radiation fluence that causes SCSI, which is about $1x10^{15}$ n/cm^2. Even after SCSI, since the n^+ strips are used as the readout electrodes, it will still be operational at partial depletion mode much beyond the SCSI. The main advantage is that cheap low resistivity wafers, especially CZ wafers with high natural oxygen concentration, can be used. The disadvantage of this p^+-n^+/n (low resistivity)/p^+ structure is that it is a double sided process, although somewhat simpler than the p^+-n^+/n/ p^+-n^+ detector since only p^+ implant will be implemented on the backside.

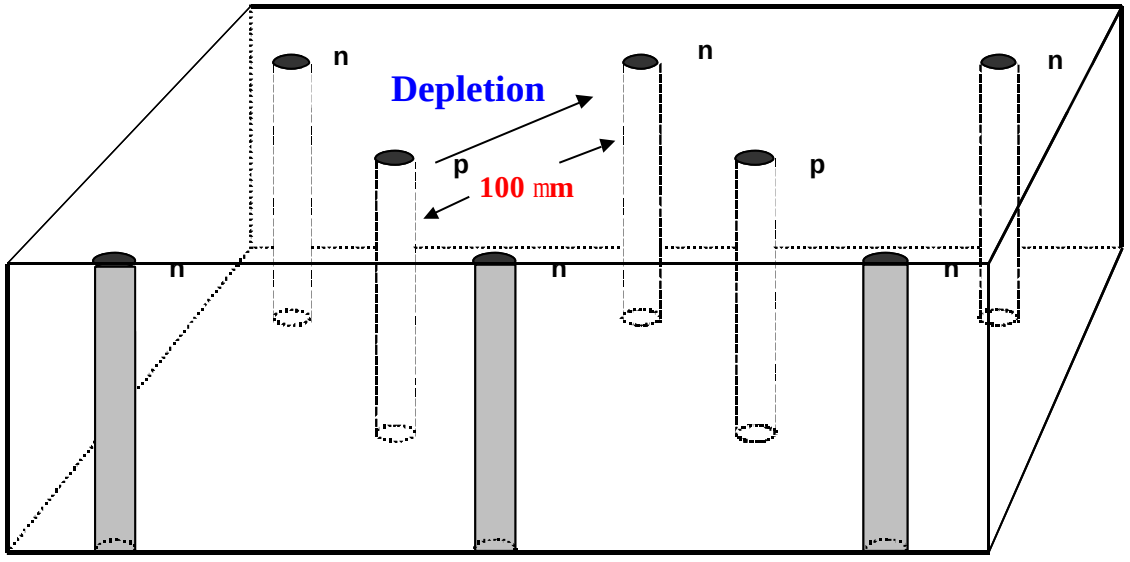

Fig. 20 Schematics of a 3D Si detector

d) Thin Detectors

One obvious and easy way to reduce the detector full depletion voltage is to reduce the detector thickness. Compare to a Si detector with standard thickness of 300 μm, a thin detector with a thickness of 50 μm can be fully depleted by a bias that is 36 times smaller, proportional to square of thickness reduction. The drawbacks for thin

detectors are: 1) signal to MIP will be reduced as well, proportional to the thickness reduction, 2) increase in detector capacitance, leading to increase in noise; and 3) decrease in signal to noise ratio. However, in some applications when

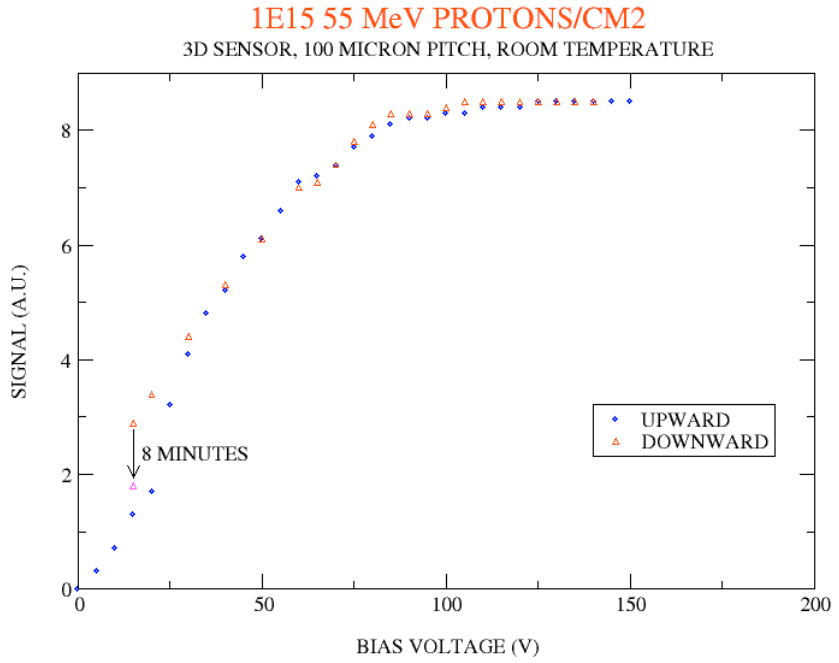

detectors with extremely high radiation tolerance, fast response, and/or extremely low mass are required, thin detectors can be one of the natural choices.

Fig. 21 CCE of a 3D Si detector irradiated by 55 MeV protons up to $1x10^{15}$ p/cm^2.

Thin detectors are more radiation tolerance. For d = 50 μm, the detector can be still fully depleted up to a fluence of $2\text{-}3x10^{15}$ n/cm^2 at a bias of 200 V: 1) for a low starting resistivity Si (50 Ω–cm) detectors, there will be no SCSI up to $1.5x10^{15}$ n/cm^2; and 2) for high starting resistivity Si (4 kΩ-cm) detectors, they can be still fully depleted up to $3x\ 10^{15}$ n/cm^2, even though SCSI taking place at about $1x10^{13}$ n/cm^2.

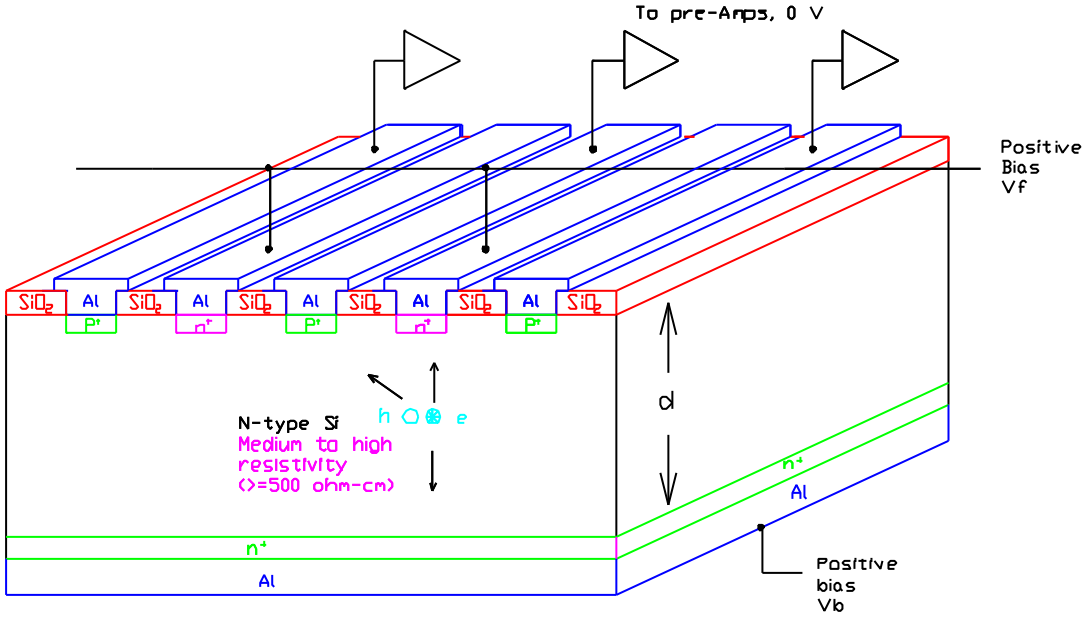

Z. Li et al, 9th Vienna Conf. on Instrumentation, Vienna, Austria, 19-23 February (2001)
Nucl. Instrum. & Meth. A478 (2002) 303-310.

Fig. 22 Schematics of a novel p^+-n^+/n/n^+ Semi-3D Si strip detector

- **Before radiation, N_{eff}= +1x10^{12} /cm^3 (4 kW-cm)**
- **Junction on the p$^+$ contacts**

Simulation, V = 100 volts

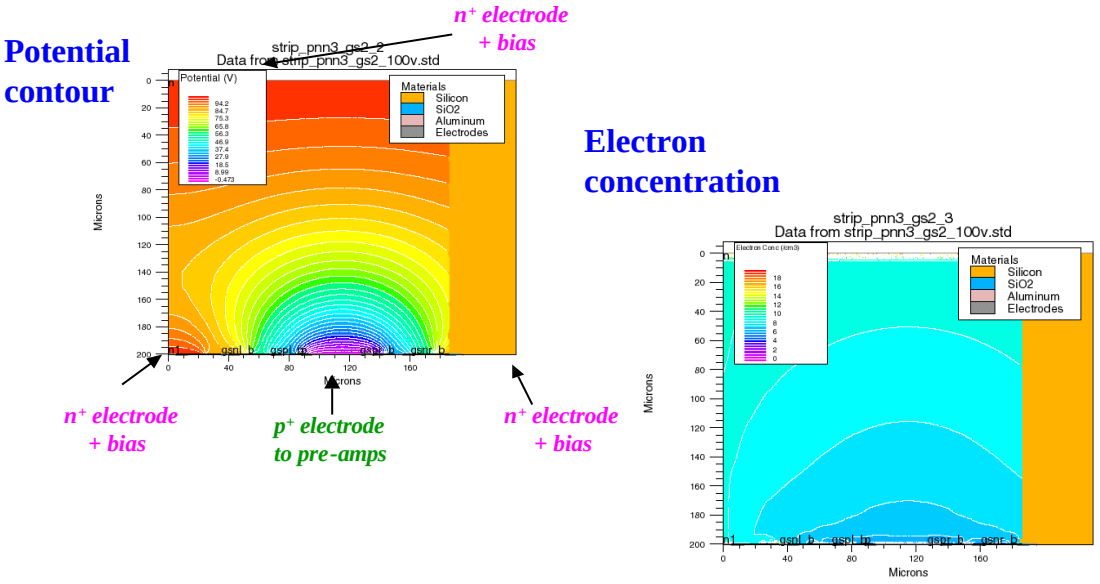

Z. Li et al, 9th Vienna Conf. on Instrumentation, Vienna, Austria, 19-23 February (2001)
Nucl. Instrum. & Meth. A478 (2002) 303-310.

Fig 23 Simulations of electric potential and electron concentration profiles of a novel p$^+$-n$^+$/n/n$^+$ Semi-3D Si strip detector before radiation.

- **After radiation, N_{eff}= -1x10^{13} /cm^3 (5x10^{14}n/cm^2)**
- **Junction on the n$^+$ contacts**

Simulation, V = 130 volts (<<370 volts)

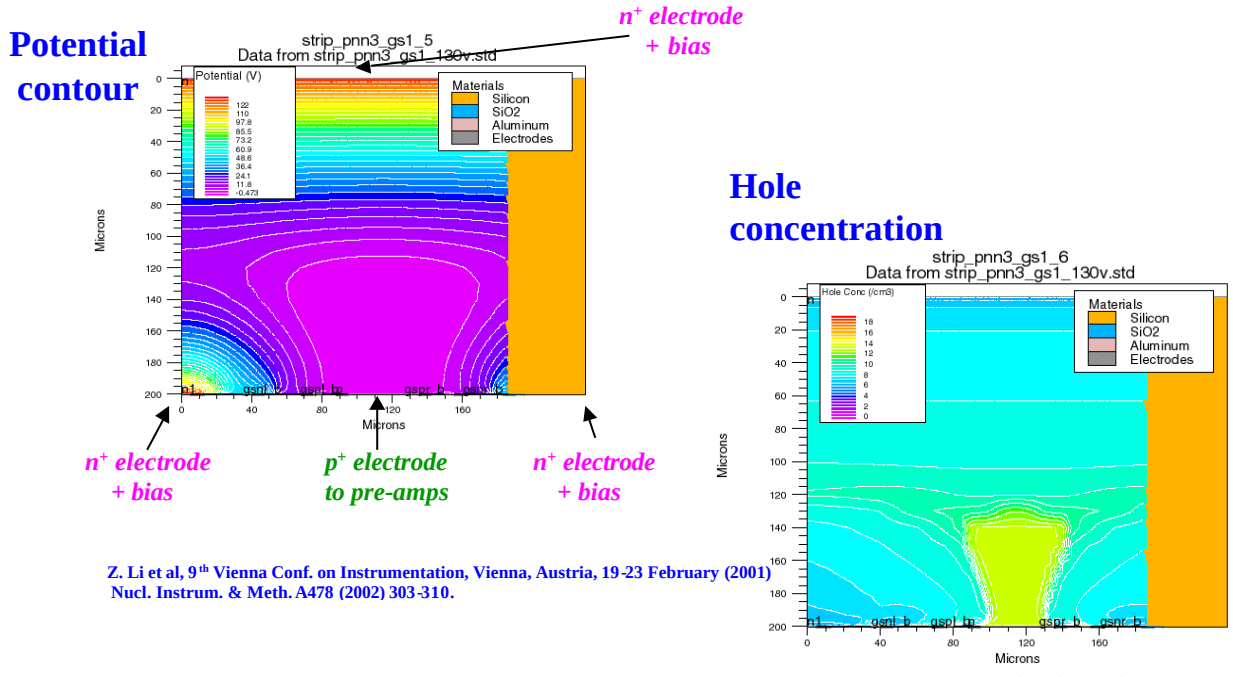

Z. Li et al, 9th Vienna Conf. on Instrumentation, Vienna, Austria, 19-23 February (2001)
Nucl. Instrum. & Meth. A478 (2002) 303-310.

Fig 24 Simulations of electric potential and hole concentration profiles of a novel p$^+$-n$^+$/n/n$^+$ Semi-3D Si strip detector after being irradiated beyond SCSI.

3. Device Operational Mode Engineering (DOME)

Sensors, when operated at different modes/conditions, it may exhibit different radiation tolerance. One of the these operational modes/conditions is sensor operation temperature. It is obvious from the results shown in Section I that low temperature operation will benefit sensor radiation hardness/tolerance. First of all, detector leakage current will be greatly diminished at low temperatures (see Fig. 3). Secondly, at a modest –10 °C, the reverse annealing effect in irradiated Si can be postponed by almost 100 years! In fact, both CMS and ATLAS at LHC will operate their detectors at temperatures < 0 °C.

The greatest benefit of cryogenic temperature operation of Si detectors was not discovered until a few years ago (1998, ref [39]) when CERN RD39 discovered the so called "Lazarus Effect": there is a significant CCE recovery at cryogenic temperatures (120 K to 150 K) for very heavily irradiated Si detectors (>10^{15} n/cm^2) that have minimum CCE at RT. As shown in Fig. 25, there are clearly CCE recovery between 120 K to 150 K for various fluences and biases [41]. In fact, operated at forward biases, detectors exhibit large and more stable CCE's. There are numerous publications by CERN RD39 on the cryogenic temperature operation, and the understanding of defect and device physics, of Si detectors [39-42], including reverse and forward bias operations, $p^+/n^+/p^+$ symmetrical detectors [42], light injected diodes (LID) [38], etc.

In fact, operating the detector at forward bias is another mode of operation. We have seen better detector performance for detectors at cryogenic temperatures [65]. Stable and better performance have also been observed for forward-biased Si detectors operated near the RT [66]. After heavy radiation, the detector bulk becomes close to intrinsic, and the bulk acts like semi-insulating material. The draw back for the forward bias operation is that it will draw huge current before or at low radiation, which complicates the detector practical operations. The $p^+/n^+/p^+$ symmetrical detectors, however, solves this problem since one of the junction is biases at reverse bias as long as the full depletion bias is not reached. After radiation beyond SCSI, the detector is basically a "resistor" like device with high bulk resistivity.

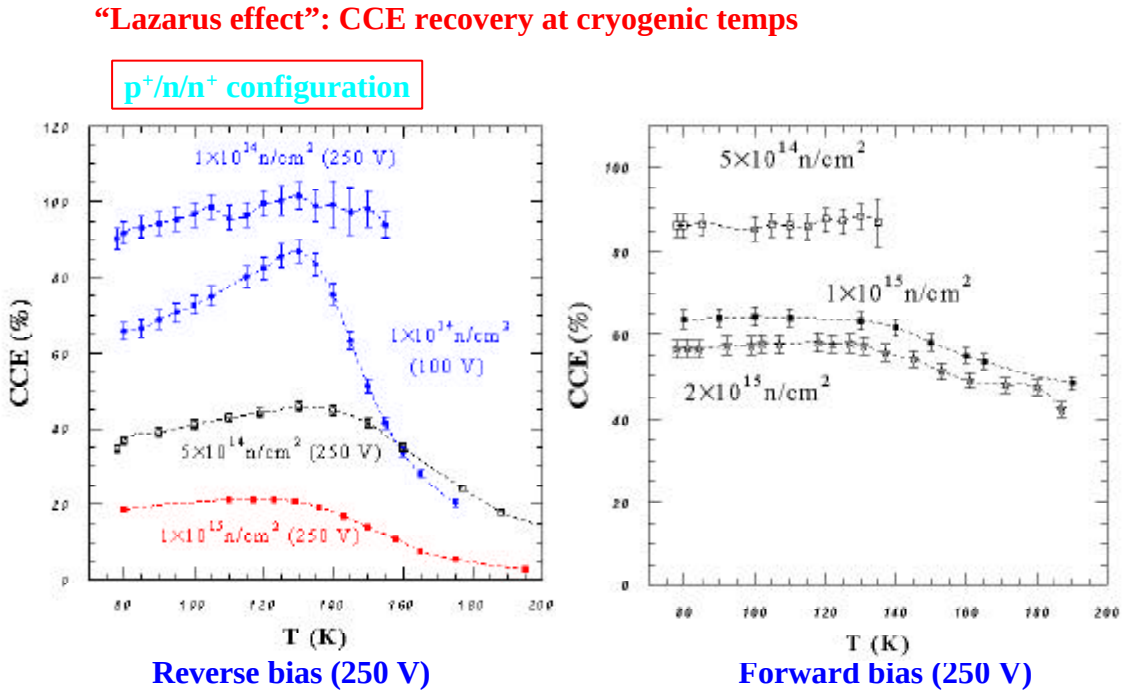

L. Casagrande, Frontier Detectors for Frontier Physics, VIII Pisa Meeting, Elba, May 2000

Fig. 25 CCE recovery at cryogenic temperatures for irradiated Si detectors.

4. New Materials (NM)

For extremely high radiation environment, say > 1x10^{16} n/cm^2, it may reach the limit of Si material working at or near room temperature (RT). Other materials, such as diamond (CERN RD42), SiC, GaN[67], etc. may have to be used. CERN RD50 already has started a program on SiC detectors, and initial results have shown great promise for using SiC as radiation detector. The 3.3 eV gap provides very low leakage current at RT and a MIP signal of about 5100 e/100 μm. Epitaxial SiC Schottky barrier detectors have been successfully tested as alpha particle detectors and

showed an 100% CCE after being irradiated by 24 GeV protons to a fluence of $1x10^{14}$ p/cm^2[68] Further tests to radiation fluences close to $1x10^{16}$ n/cm^2 are in the plan for the coming year.

IV. Future Trends

In pushing the radiation hardness/tolerance limit of Si detector and other semiconductor detectors operating at or near RT, the following tasks may be carried out in the coming years: MIDE --- O and other impurities: H, Cl, N, oxygen-dimers [69], etc. will be studied in detail

2 DSE --- Realize 3D and semi-3D detectors, and thin detectors: prototypes and full detectors
(These two tasks may push rad-hardness/tolerance of Si detectors to a few times of $1x10^{15}$ n/cm^2)

3 Make detectors with combined technologies:
(This may push rad-hardness/tolerance of Si detectors close to 10^{16} n/cm^2)

- a Oxygenated detectors with MGS and/or 3D and Semi-3D detector structures
- b Oxygenated low resistivity detectors with MGS and/or 3D and Semi-3D detector structures
- c Oxygenated detectors operated at cryogenic temperatures/forward biases
- d 3D and Semi-3D detector structures operated at cryogenic temperatures
- e Other possible combinations

4 Other semiconductor materials for extremely high radiation, SiC, etc.
(This may push detector rad-hardness/tolerance over 10^{16} n/cm^2)

V. Summary

The details in displacement radiation damage in Si sensors have been reviewed in this paper. The main radiation induced damage in Si sensors and degradations in sensor performances can be summarized as the following:

1. The displacement radiation induced damage in Si is mainly in the form of deep level single defects and defect clusters (extended defect regions). For neutron radiation, it is mainly in the form of defect clusters. For gamma and electron radiations, it is mainly in the form of deep level single defects. For charge particles (protons, pions, etc.), it is the mixture of the two.
2. The first and most obvious radiation damage effect on Si sensor is the increase of sensor leakage current with the radiation fluence. For 1 MeV equivalent neutron fluence, the increase in volume current is proportional to the fluence. The proportional constant or the damage constant, α, is within $4\text{-}6x10^{-17}$ A/cm at 20 °C for high resistivity Si (2-8 kΩ-cm). The cause for the leakage current increase is the thermal generation of carriers from radiation induced deep level defects and defect clusters.
3. For the neutral bulk Si, the displacement damage is mainly reflected in the increase of bulk resistivity towards the intrinsic value (200 k to 300 k Ω-cm) and increase in carrier Hall mobility.
4. The space charge in the depletion region of the Si sensors undergoes various transformations during radiation, anneal, and operation:

Although radiation induced damage/degradation in Si sensors is quite extensive and severe, Si sensors can be, however, made more radiation hard/tolerant by employing three different engineering technologies: Material/Impurity/Defect Engineering (MIDE), Device Structure Engineering (DSE), and Device Operational Mode Engineering (DOME). Sensor radiation hardness/tolerance can be improved by a factor from 2 to 4 for a giving technology. With possible combinations of different technologies, the radiation hardness of Si detectors may be improved by a factor of more than 10, making them suitable to the application of future LHC Upgrades. For even higher radiation environments where fluences > 10^{16} n/cm^2 are present, other semiconductor materials, such as SiC, may be used as detector materials.

Acknowledgements

The author would like to thank our collaborators from Beijing Institute of Semiconductors, BNL (AGS, NSLS, Physics, RHIC (STAR)), CERN (RD39, NA60, RD50); FNAL, JHU, Ioffe Physico-Technical Institute, LANL, Purdue

University, UC Davis, University of Florence, University of Hamburg, University of Roma I, and Wayne State University for their contributions during various collaborating projects. This research was supported by the U.S. Department of Energy: contract No: DE-AC02-98ch10886, and was done partially within the framework of CERN RD50 Collaboration and partially within the framework of CERN RD39 Collaboration.

VI. References

1. CMS Technical Proposal, CERN/LHCC/94-38, 1994.

2. ATLAS technical Proposal, CERN/LHCC 94-43, LHCC/P2, 1994.

3. V.A.J. van Lint, "The physics of radiation damage in particle detectors", Nucl. Instr. & Meth., A253, 453 (1987).

4. H. W. Kraner et al., Nucl. Instrum. & Meth. A279, 266-271 (1989).

5. Zheng Li et al., IEEE Trans. Nucl. Sci. NS-39, No. 6 1730-1738 (1992).

6. E. Verbitskaya, et al, Presented at the 3rd Conference on Radiation Effects on Semiconductor Materials, Detectors and Devices, Florence, Italy, July 20007. Z. Li, et al, Nucl. Inst. &d Meth., A308, 585 (1991)

M. Moll, Ph.D. Thesis, University of Hamburg, 1999, DESY THESIS-1999-040, ISSN-1435-80859. B. Dezillie et al., IEEE Trans. Nucl. Vol. 46, No. 3, 221 (1999) 10. S. Pirollo et al., Nucl. Inst. & Meth., A426, 126-130 (1999) 11. V. Eremin and Z. Li, IEEE Trans. Nucl. Vol. 41, No. 6, 1907 (1994) 12. R. Wunstorf, Ph.D. Thesis, University of Hamburg, 1992, DESY FH1K-92-01. 13. Z. Li and H.W. Kraner, Nucl. Phys. B, 32 398-409 (1993)

14. B. Dezillie, Z. Li et al., IEEE Trans. Nucl. Vol. 46, No. 3, 221 (1999)

15. Z. Li and H.W. Kraner, Nucl. Phys. B, 32, 398-409 (1993)

16. H. Kraner et al, Nucl. Instrum. & Meth. A326, 398-405 (1993)

17. G. Kramberger, presented at CERN RD48 Workshop, Geneva, March, 2000

18. A. Chilingarov, presented at CERN RD48 Workshop, Geneva, March, 2000

19. T.J. Brodbeck et al., Nucl. Instrum. & Meth. A455, 645-655 (2000)
20. G. Kramberger, Ph.D. Thesis, University of Ljubljana, 2001
21. G. Kramberger et al., Nucl. Instrum. & Meth. A76, 645-651 (2002)
22. G. Kramberger et al, IEEE Trans. Nucl. Sci., Vol. 49, No. 4, 2002 (in press)

23. Z. Li et al., IEEE Trans. Nucl. Sci., Vol. 42, No. 4, 219 (1995) 24. Z. Li et al., Nucl. Instrum. & Meth. A377, 265-275 (1996).

25. Z. Li, IEEE Trans. Nucl. Sci., Vol. 42, No. 4, 224 (1995)

26 Z. Li et al.; IEEE Trans. Nucl. Sci. NS-44, No. 3, 834 (1997)

27. G. Casse, presented at the 1st Workshop on Radiation Hard Semiconductor Devices for High Luminosity Colliders, CERN, Geneva, 28030, Nov. 2002

28. V. Cindro et al., Nucl. Instrum. & Meth. A450 288 (2000)

Nucl. Instrum. & Meth. A466 345 (2001)

V. Cindro et al., Nucl. Instrum. & Meth. A76 562-568 (2002)

35. V. Eremin, Z. Li, and Ijashenko; Nucl. Instrum. & Meth. A360 458 (1995)

36. Z. Li et al., Nucl. Inst. & Meth., A388 297-307 (1997)

37. E. Verbitskaya et al, IEEE Trans. Nucl. Sci, vol. 49, No. 1, 258-263 (2002)

38. M. Zavrtanik et al., IEEE Trans. Nucl. Sci. Vol. 49, No. 1, 264-269 (2002)

39 V. Palmieri et al., Nucl. Inst. & Meth., A413 475 (1998).40 RD39 Collaboration, K. Borer et al., CERN/LHCC98-27, DRDC P53 Add. 1(1998).

41. L. Casagrande et al., Nucl. Inst. & Meth., A461, 150-154 (2001).42. K. Borer et al., Nucl. Inst. & Meth., A462, 474-483 (2001).43. Z. Li and H.W. Kraner, J. Electronic Materials, Vol. 21, No. 7, 701 (1992) 44. D. Menichelli et al., Nucl. Inst. & Meth., A426, 135-139 (1999)

45. V. Eremin, et al., Nucl. Inst. & Meth., A476, 556-564 (2002)

46. B. MacEvoy, 3rd ROSE Workshop 12-14 Feb 9847. S. Lazanu et al., RESMDD02, Florence, Italy, July 10-12, 2002

48. Z. Li et al., IEEE Trans. Nucl. Sci., Vol. 39, No. 6, (1992) 1730 49. A. Ruzin and CERN Rd48 Collaboration, Nucl. Instrum. & Meth. A447, 116-125 (2000)

50 RD48 Status Report, CERN/LHCC 2000-009, December 1999.

51 G. Lindstroem and CERN RD48 Collaboration, Nucl. Instrum. & Meth. A466, 308 (2001)

52. G. Lindstroem, presented at the 9th European Syposium on Semiconductor Detectors, Schloss Elmau, June 23-27, 2002, to be published in Nucl. Instrum. & Meth. A.

53. B. Dezillie et al, IEEE Trans. Nucl. Sci., Vol. 47, No. 6, 1892-1897 (2000)

54. Z. Li et al, RESMDD02, Florence, Italy, July 10-12, 2002, to be published in Nucl. Instrum. & Meth. A

55. E. Fretwurst et al, RESMDD02, Florence, Italy, July 10-12, 2002, to be published in Nucl. Instrum. & Meth. A

56. Z. Li et al., Nucl. Inst. & Meth., A461 (2001) 126-132

57. M. Huhtinen, ROSE/TN/2001-02, to be published in Nucl. Instrum. & Meth. A

RESMDD02, Florence, Italy, July 10-12, 2002, to be published in Nucl. Instrum. & Meth. A

60. Z. Li et al., Nucl. Instrum. & Meth. A409 (1998) 180.

61. H.S. Cho et al., IEEE Trans. Nucl. Sci. Vol. 47, No. 3, June (2000) 772-776

62. G. Bolla et al., Nucl. Instrum. & Meth. A435 (1999) 178-186.

63. Sherwood I. Parker et al., UH 511-959-00 (2000)

Z. Li et al, 9th Vienna Conf. on Instrumentation, Vienna, Austria, 19-23 February (2001); Nucl. Instrum. & Meth. A478 (2002) 303-310.

65. K.Borer et al.; Nucl. Instrum. & Meth. A440, 5-16 (2000)

66. L. Beattie et al Nucl. Instrum. & Meth. A439, 293-300 (2000)

67. J. Vaitkus et al., Proc. 4th Intern.Workshop on Radiation Imaging Detectors, 2002, Amsterdam. To be published in NIM-A.68. M. Bruzzi et al, IEEE Nucl. Sc. Sym., Norfolk, VA, Nov. 10 to 16, 2002.

69. C. DaVia and S. Watts, Nucl. Instrum. & Meth. B186, 111 (2002)